# Buckling behavior of smart MEE-FG porous plate with various boundary conditions based on refined theory

Farzad Ebrahimi[*] and Ali Jafari

*Department of Mechanical Engineering, Faculty of Engineering, Imam Khomeini International University, Qazvin, Iran*

**Abstract.** Present disquisition proposes an analytical solution method for exploring the buckling characteristics of porous magneto-electro-elastic functionally graded (MEE-FG) plates with various boundary conditions for the first time. Magneto electro mechanical properties of FGM plate are supposed to change through the thickness direction of plate. The rule of power-law is modified to consider influence of porosity according to two types of distribution namely even and uneven. Pores possibly occur inside FGMs due the result of technical problems that lead to creation of micro-voids in these materials. The variation of pores along the thickness direction influences the mechanical and physical properties. Four-variable tangential-exponential refined theory is employed to derive the governing equations and boundary conditions of porous FGM plate under magneto-electrical field via Hamilton's principle. An analytical solution procedure is exploited to achieve the non-dimensional buckling load of porous FG plate exposed to magneto-electrical field with various boundary condition. A parametric study is led to assess the efficacy of material graduation exponent, coefficient of porosity, porosity distribution, magnetic potential, electric voltage, boundary conditions, aspect ratio and side-to-thickness ratio on the non-dimensional buckling load of the plate made of magneto electro elastic FG materials with porosities. It is concluded that these parameters play remarkable roles on the dynamic behavior of porous MEE-FG plates. The results for simpler states are confirmed with known data in the literature. Presented numerical results can serve as benchmarks for future analyses of MEE-FG plates with porosity phases.

**Keywords:** buckling analysis; MEE-FG plate; porous materials; refined plate theory

## 1. Introduction

Magneto-electro-elastic materials (MEEMs) as one of the special sorts of smart materials have received much attention in engineering structures during the recent years. In 1990s, in two-phase composites of piezoelectric and piezo-magnetic materials, a strong magneto-electrical coupling effect was discovered which has potential practical application in many fields (Harshe *et al*. 1993, Zeng *et al*. 2014) and reported that this coupling effect cannot be found in a single-phase material. Furthermore, MEE materials shows some fascinating properties such as the piezo-electric,

---

*Corresponding author, Ph.D., E-mail: febrahimy@ut.ac.ir

piezo-magnetic and magneto-electric influences in which the elastic deformations may be produced directly by mechanical loading or indirectly by an application of electric or magnetic field. The mechanical behaviors of magneto-electro-elastic structures have received notable attention by many researchers in the recent years. Among them, analytical solutions for studying magneto-electro-elastic responses of beams is presented by Jiang and Ding (2004). Chen *et al.* (2005) investigated vibrational responses of non-homogeneous isotropic MEE plates. Also, Liu and Chang (2010) provided closed solution for the vibration of an isotropic magneto-electro-elastic plate. Most recently, based on three-dimensional elasticity theory and employing the state space approach, Xin and Hu (2015) presented semi-analytical evaluation of free vibration of arbitrary layered magneto-electro-elastic beams.

Functionally graded materials (FGMs) as a new class of composite structures have drawn the attention of many researchers in the smart materials and structures by minimizing or removing stress concentrations at the interfaces of the traditional composite materials. The material properties of FGMs varies continuously in one or more directions (Ebrahimi *et al.* 2009, Ebrahimi and Rastgoo 2009, 2011, Aghelinejad *et al.* 2011). Recently, FGMs have received wide applications as structural components in modern industries such as mechanical, civil, nuclear reactors, and aerospace engineering. In the recent years, several researchers examined mechanical properties of structural elements made from magneto-electro-elastic functionally graded (MEE-FG) materials. Some of researchers in recent years have analyzed mechanical behaviors of FGM nanoplates based on various plate shear deformation plate theories. (Ebrahimi and Barati 2016 a, b, c, d, e, Ebrahimi *et al.* 2016a, Ebrahimi and Dabbagh 2016, Ebrahimi and Hosseini 2016 a, b). Also analysis of nano-structure's mechanical behaviors is one of recent interesting research topics. (Ebrahimi and Barati, 2016 f-n, Ebrahimi and Barati 2017). Thermal buckling and free vibration analysis of FG nanobeams subjected to temperature distribution have been exactly investigated by Ebrahimi and Salari (2015 a-c) and Ebrahimi *et al.* (2015 a, b). Ebrahimi and Barati (2016 o, p, q) investigated buckling behavior of smart piezoelectrically actuated higher-order size-dependent graded nanoscale beams and plates in thermal environment. Pan and Han (2005) provided exact solution for analysis of the rectangular plates composed of functionally graded, anisotropic, and linear magneto-electro-elastic materials. Furthermore, the plane stress problem of a MEE-FG beam were inspected by Huang, Ding *et al.* (2007) using an analytical method. Kattimani and Ray (2015) researched large amplitude vibration responses of MEE-FG plates. Static behavior of a circular MEE-FG plate is analyzed by Sladek, Sladek *et al.* (2015) by using a meshless method.

With the rapid progression in technology of structural elements, structures with graded porosity can be introduced as one of the latest development in FGMs. The structures consider pores into microstructures by taking the local density into account. Researches focus on development in preparation methods of FGMs such as powder metallurgy, vapor deposition, self-propagation, centrifugal casting, and magnetic separation. These methods have their own ineffectiveness such as high costs and complexity of the technique. An efficient way to manufacture FGMs is sintering process in which due to difference in solidification of the material constituents, porosities or micro-voids through material can create (Zhu *et al.* 2001). An investigation has been carried out on porosities existing in FGMs fabricated by a multi-step sequential infiltration technique (Wattanasakulpong *et al.* 2012). According to this information about porosities in FGMs, it is necessary to study the porosity impact when designing and analyzing FGM structures. Porous FG structures have many interesting combinations of mechanical properties, such as high stiffness in conjunction with very law specific weight (Rezaei and Saidi 2016). A few investigations on the mechanical responses of porous FG structures are available in literature. Wattanasakulpong and
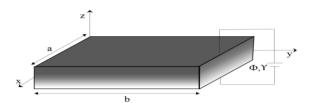
Fig. 1 Geometry of FGM plate under magneto-electrical field

Ungbhakorn (2014) studied the linear and non-linear vibration of porous FGM beams with elastically restrained ends. In order to predict flexural vibration of porous FGM Timoshenko beams, Wattanasakulpong and Chaikittiratana (2015) employed Chebyshev collocation method. Moreover, Yahia *et al.* (2015) study the porosity effect on the wave propagation of FG plates by using various higher-order shear deformation theories. Ebrahimi *et al.* (2016) presented thermo-mechanical vibration response of temperature-dependent porous FG beams subjected to various temperature risings. Recently, Mechab *et al.* (2016) developed a nonlocal elasticity model for free vibration of FG porous nanoplates resting on elastic foundations. Boutahar and Benamar (2016) presented a semi analytical method for non-linear vibration analysis of FGM porous annular plates resting on elastic foundations. Recently, it is well understood that classic plate theory (CPT) is not appropriate for thick beams and higher modes of vibration. This is because of CPT ignores the impact of the shear deformation. Hereupon, first order shear deformation theory (FSDT) is suggested to overcome the defects of CPT with supposition a shear correction factor in the thickness direction of beam. As regards FSDT isn't able to evaluate the zero-shear stress on the top and bottom surfaces of the plate, there appeared a need to develop higher order theory (HOT). This theory doesn't need any shear correction factors and predict transverse shear stresses properly. Many papers are published which utilize HOT to investigate mechanical response of FG structures (Larbi *et al.* 2013, Atmane *et al.* 2015, Nguyen *et al.* 2015, Vo *et al.* 2015). One of the main mechanical characteristics of FGM structures is the buckling response which play a notable role on the safety of engineering structures, and accordingly has received intense attention by several researchists (Ke *et al.* 2012, Şimşek and Yurtcu 2013). Therefore, With the wide application of magneto electro porous FG structures, understanding buckling of MEE-FG plate with porosities becomes an important task.

From the literature mentioned above, it is apparent that no paper published in the title of buckling of MEE-FG porous plate. According to wide application of magneto electro elastic porous FG structures, understanding buckling behavior of MEE-FG plate with porosities becomes important issue. The main incentive of this paper is to develop an analytical solution for examining the buckling behavior of smart FG porous plate under magnetic and electric field with various boundary conditions based on refined plate theory. The modified power-law model is exploited to describe gradual variation of magneto electro mechanical material characteristics of porous MEE-FG plate with two porosity distributions (even & uneven). Applying Hamilton's principle, governing equations of higher order MEE-FG plate are obtained together based on four-variable refined shear deformation theory and they are solved applying an analytical solution method. Several numerical exercises are presented investigating the influences of porosity, type of porous distribution, external electric voltage, magnetic potential, material graduation index, Side-to-thickness ratio, aspect ratio and boundary condition on the buckling behavior of MEE-FG porous plate.

Table 1 Magneto-electro-elastic coefficients of material properties (Ramirez *et al.* 2006)

| Properties | BaTiO$_3$ | CoFe$_2$O$_4$ | Properties | BaTiO$_3$ | CoFe$_2$O$_4$ | Properties | BaTiO$_3$ | CoFe$_2$O$_4$ |
|---|---|---|---|---|---|---|---|---|
| $c_{11}=c_{22}$ (GPa) | 166 | 286 | $e_{15}$ | 11.6 | 0 | $\rho\,(\mathrm{kg\,m^{-3}})$ | 5800 | 3005 |
| $c_{33}$ | 162 | 269.5 | $q_{31}$ (N/Am) | 0 | 580.3 | $d_{11}=d_{22}=d_{33}$ | 0 | 0 |
| $c_{13}=c_{23}$ | 78 | 170.5 | $q_{33}$ | 0 | 699.7 | $\chi_{33}$ | 10 | 157 |
| $c_{12}$ | 77 | 173 | $q_{15}$ | 0 | 550 | $e_{33}$ | 18.6 | 0 |
| $c_{55}$ | 43 | 45.3 | $s_{11}\,(10^{-9}\mathrm{C^2\,m^{-2}\,N^{-1}})$ | 11.2 | 0.08 | $s_{33}$ | 12.6 | 0.093 |
| $c_{66}$ | 44.5 | 56.5 | $\chi_{11}(10^{-6}\,Ns^2\mathrm{C}^{-2}/2)$ | 5 | -590 | $e_{31}(cm^{-2})$ | -4.4 | 0 |



(a) even                                    (b) uneven
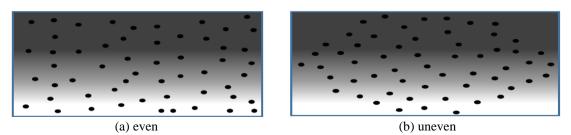
Fig. 2 Cross-section area of FGM plate with even and uneven porosities

## 2. Theoretical formulations

### 2.1 The material properties of porous magneto-electro-elastic FG plates

Consider a magneto-electro-elastic functionally graded plate with two different porosity distribution and rectangular cross-section of width *b* and thickness *h* according to Fig. 1. MEE-FG plate is composed of BaTio$_3$ and CoFe$_2$O$_4$ materials with the material properties presented in Table 1 and exposed to a magnetic potential $\gamma(\chi,z,t)$ and electric potential $\Phi(\chi,z,t)$. The effective material properties of MEE-FG plate change continuously in the thickness direction according to modified power-law distribution. The effective material properties $(P_f)$ of porous FGM plate by using the modified rule of mixture can be expressed by Wattanasakulpong and Ungbhakorn (2014)

$$P_f = P_u(V_u - \frac{\alpha}{2}) + P_l(V_l - \frac{\alpha}{2}) \tag{1}$$

In which $\alpha$ denotes the volume fraction of porosities, $P_u$, $V_u$ and $V_l$ are the material properties and volume fraction of top and bottom sides, respectively and are related by

$$V_u + V_l = 1 \tag{2}$$

Then the volume fraction of upper side $(V_u)$ is defined as follows

$$V_u = (\frac{z}{h} + \frac{1}{2})^P \tag{3}$$

Where $(p \geq 0)$ is a non-negative parameter (power-law exponent or the volume fraction index) which determine the material distribution across the plate thickness.

$$P(z) = (P_u - P_l)\left(\frac{z}{h} + \frac{1}{2}\right)^p + P_l - (P_u + P_l)\frac{\alpha}{2} \tag{4}$$

The MEE-FG (II) plate has porosity phases spreading frequently nearby the middle zone of the cross-section and the amount of porosity seems to be linearly decrease to zero at the top and bottom of the cross-section. Fig. 2 demonstrates cross-section areas of FGM-I and-II with porosities phases. The effective material properties of MEE-FG (II) are replaced by following form.

$$P(z) = (P_u - P_l)\left(\frac{z}{h} + \frac{1}{2}\right)^p + P_l - \frac{\alpha}{2}(P_u + P_l)(1 - \frac{2|z|}{h}) \tag{5}$$

## 2.2 Inematic relations

Based on new tangential-exponential refined shear deformation theory, the displacement field at any point of the plate can be expressed as

$$u_1(x, y, z, t) = u(x, y, t) - z\frac{\partial w_b}{\partial x} - f(z)\frac{\partial w_s}{\partial x} \tag{6}$$

$$u_2(x, y, z, t) = v(x, y, t) - z\frac{\partial w_b}{\partial y} - f(z)\frac{\partial w_s}{\partial y} \tag{7}$$

$$u_3(x, y, z, t) = w_b(x, y, t) + w_s(x, y, t) \tag{8}$$

Which $u$ and $v$ are displacement of mid-plane along $x$, y-axis and are the bending and shear components of transverse displacement of a point on the mid-plane of the plate and $t$ is the time. $f(z)$ denotes a shape function estimating the distribution of shear stress across the plate thickness. $f(z)$ is considered to satisfy the stress-free boundary conditions on the top and bottom sides of the plate. So, it is not required to use any shear correction factor. The present theory has a function in the form Mantari *et al.* (2014)

$$f(z) = \tan(\frac{\pi z}{2h})r^{\sec(\frac{\pi z}{2h})}, \quad r = 0.03 \tag{9}$$

The electric potential and magnetic potential distributions across the thickness are approximated via a combination of a cosine and linear variation to satisfy Maxwell's equation in the quasi-static approximation as follows (Ke and Wang 2014)

$$\Phi(x, y, z, t) = -\cos(\xi z)\phi(x, y, t) + \frac{2z}{h}V \tag{10}$$

$$\Upsilon(x, y, z, t) = -\cos(\xi z)\gamma(x, y, t) + \frac{2z}{h}\Omega \tag{11}$$

Where $\xi = \pi/h$. Also, $v$ and $\Omega$ are the external electric voltage and magnetic potential applied to the MEE-FG plate. Nonzero strains of the four-variable plate model are expressed by

$$\begin{Bmatrix} \varepsilon_x \\ \varepsilon_y \\ \gamma_{xy} \end{Bmatrix} = \begin{Bmatrix} \varepsilon_x^0 \\ \varepsilon_y^0 \\ \gamma_{xy}^0 \end{Bmatrix} + z \begin{Bmatrix} \kappa_x^b \\ \kappa_y^b \\ \kappa_{xy}^b \end{Bmatrix} + f \begin{Bmatrix} \kappa_x^s \\ \kappa_y^s \\ \kappa_{xy}^s \end{Bmatrix}, \begin{Bmatrix} \gamma_{yz} \\ \gamma_{xz} \end{Bmatrix} = g \begin{Bmatrix} \gamma_{yz}^s \\ \gamma_{xz}^s \end{Bmatrix}, g = 1 - \frac{\partial f}{\partial z} \tag{12}$$

Where

$$\begin{Bmatrix} \varepsilon_x^0 \\ \varepsilon_y^0 \\ \gamma_{xy}^0 \end{Bmatrix} = \begin{Bmatrix} \frac{\partial u}{\partial x} \\ \frac{\partial v}{\partial y} \\ \frac{\partial u}{\partial y} + \frac{\partial v}{\partial x} \end{Bmatrix}, \begin{Bmatrix} \kappa_x^b \\ \kappa_y^b \\ \kappa_{xy}^b \end{Bmatrix} = \begin{Bmatrix} -\frac{\partial^2 w_b}{\partial x^2} \\ -\frac{\partial^2 w_b}{\partial y^2} \\ -2\frac{\partial^2 w_b}{\partial x \partial y} \end{Bmatrix}, \begin{Bmatrix} \kappa_x^s \\ \kappa_y^s \\ \kappa_{xy}^s \end{Bmatrix} = \begin{Bmatrix} -\frac{\partial^2 w_s}{\partial x^2} \\ -\frac{\partial^2 w_s}{\partial y^2} \\ -2\frac{\partial^2 w_s}{\partial x \partial y} \end{Bmatrix}, \begin{Bmatrix} \gamma_{yz}^s \\ \gamma_{xz}^s \end{Bmatrix} = \begin{Bmatrix} \frac{\partial w_s}{\partial y} \\ \frac{\partial w_s}{\partial x} \end{Bmatrix} \tag{13}$$

According to Eq. (10), the relation between electric field ($E_\chi, E_y, E_z$) and electric potential, ($\Phi$) can be obtained as

$$\{E_x, E_y\} = \{-\Phi_{,x}, -\Phi_{,y}\} = \cos(\xi z)\{\frac{\partial \phi}{\partial x}, \frac{\partial \phi}{\partial y}\} \tag{14}$$

$$E_z = -\Phi_{,z} = -\xi \sin(\xi z)\phi - \frac{2v}{h}, \tag{15}$$

Also, the relation between magnetic field ($H_x, H_y, H_z$) and magnetic potential ($\Upsilon$) can be expressed from Eq. (11) as

$$\{H_x, H_y\} = \{-\Upsilon_{,x}, -\Upsilon_{,y}\} = \cos(\xi z)\{\frac{\partial \gamma}{\partial x}, \frac{\partial \gamma}{\partial y}\} \tag{16}$$

$$H_z = -\Upsilon_{,z} = -\xi \sin(\xi(z))\gamma - \frac{2\Omega}{h} \tag{17}$$

Through extended Hamilton's principle, the equation of motion can be derived by

$$\int_0^t \delta(\Pi_S + \Pi_W) dt = 0 \tag{18}$$

Here $\prod_s$ is strain energy, $\prod_W$ is work done by external forces. The following Euler-Lagrange equations are obtained bu utilizing the virtual work principle and setting the coefficints of $\delta u$, $\delta v$, $\delta w_b$, $\delta w_s$, $\delta \phi$ and $\delta \gamma$ are equal to zero

$$\frac{\partial N_x}{\partial x} + \frac{\partial N_{xy}}{\partial y} = 0 \tag{19}$$

$$\frac{\partial N_{xy}}{\partial x} + \frac{\partial N_y}{\partial y} = 0 \tag{20}$$

$$\frac{\partial^2 M_x^b}{\partial x^2} + 2\frac{\partial^2 M_{xy}^b}{\partial x \partial y} + \frac{\partial^2 M_y^b}{\partial y^2} - (N^b + N^E + N^H)\nabla^2(w_b + w_s) = 0 \tag{21}$$

$$\frac{\partial^2 M_x^s}{\partial x^2} + 2\frac{\partial^2 M_{xy}^s}{\partial x \partial y} + \frac{\partial^2 M_y^s}{\partial y^2} + \frac{\partial Q_{xz}}{\partial x} + \frac{\partial Q_{yz}}{\partial y} - (N^b + N^E + N^H)\nabla^2(w_b + w_s) = 0 \tag{22}$$

$$\int_{-h/2}^{h/2}\left(\cos(\xi z)\frac{\partial D_x}{\partial x} + \cos(\xi z)\frac{\partial D_y}{\partial y} + \xi\sin(\xi z)D_z\right)dz = 0 \tag{23}$$

$$\int_{-h/2}^{h/2}\left(\cos(\xi z)\frac{\partial B_x}{\partial x} + \cos(\xi z)\frac{\partial B_y}{\partial y} + \xi\sin(\xi z)B_z\right)dz = 0 \tag{24}$$

Which the variables introduced at the last expression are expressed by

$$(N_i, M_i^b, M_i^s) = \int_A (1, z, f)\sigma_i \, dA, \, i = (x, y, xy) \tag{25}$$

$$Q_i = \int_A g\sigma_i \, dA, \, i = (xz, yz) \tag{26}$$

For a linear MEE porous FG plate exposed to magneto-electro-mechanical loading, the coupled constitutive relations may be rewritten as

$$\sigma_{ij} = C_{ijkl}\varepsilon_{kl} - e_{mij}E_m - q_{nij}H_n \tag{27}$$

$$D_i = e_{ikl}\varepsilon_{kl} + k_{im}E_m + d_{in}H_n \tag{28}$$

$$B_i = q_{ikl}\varepsilon_{kl} + d_{im}E_m + \chi_{in}H_n \tag{29}$$

Which $\sigma_{ij}$, $D_i$, $B_i$ denotes the components of stress, electric displacement and magnetic induction, $\varepsilon_{kl}$, $E_m$ and $H_n$ are the components of linear strain, electric field and magnetic field. Additionally, $C_{ijkl}$, $k_{im}$ and $\chi_{in}$ are the components of elastic stiffness, dielectric permittivity and magnetic permittivity coefficients; Finally, $e_{mij}$, $q_{nij}$ and $d_{in}$ are the piezoelectric, piezo-magnetic, and magneto-electric-elastic coefficients, respectively. By integrating Eqs. (27)-(29) over the area of MEE porous FG plate cross-section, the following relations for the force-strain and the moment-strain and other necessary relation of the refined FG plate can be obtained

$$\begin{Bmatrix} N_x \\ N_y \\ N_{xy} \end{Bmatrix} = \begin{pmatrix} A_{11} & A_{12} & 0 \\ A_{12} & A_{22} & 0 \\ 0 & 0 & A_{66} \end{pmatrix}\begin{Bmatrix} \frac{\partial u}{\partial x} \\ \frac{\partial v}{\partial y} \\ \frac{\partial u}{\partial y}+\frac{\partial v}{\partial x} \end{Bmatrix} + \begin{pmatrix} B_{11} & B_{12} & 0 \\ B_{12} & B_{22} & 0 \\ 0 & 0 & B_{66} \end{pmatrix}\begin{Bmatrix} -\frac{\partial^2 w_b}{\partial x^2} \\ -\frac{\partial^2 w_b}{\partial y^2} \\ -2\frac{\partial^2 w_b}{\partial x \partial y} \end{Bmatrix} + \begin{pmatrix} B_{11}^s & B_{12}^s & 0 \\ B_{12}^s & B_{22}^s & 0 \\ 0 & 0 & B_{66}^s \end{pmatrix}\begin{Bmatrix} -\frac{\partial^2 w_s}{\partial x^2} \\ -\frac{\partial^2 w_s}{\partial y^2} \\ -2\frac{\partial^2 w_s}{\partial x \partial y} \end{Bmatrix} + \begin{Bmatrix} A_{31}^e \\ A_{31}^e \\ 0 \end{Bmatrix}\phi + \begin{Bmatrix} A_{31}^m \\ A_{31}^m \\ 0 \end{Bmatrix}\gamma \tag{30}$$

$$\begin{Bmatrix} M_x^b \\ M_y^b \\ M_{xy}^b \end{Bmatrix} = \begin{pmatrix} B_{11} & B_{12} & 0 \\ B_{12} & B_{22} & 0 \\ 0 & 0 & B_{66} \end{pmatrix}\begin{Bmatrix} \frac{\partial u}{\partial x} \\ \frac{\partial v}{\partial y} \\ \frac{\partial u}{\partial y}+\frac{\partial v}{\partial x} \end{Bmatrix} + \begin{pmatrix} D_{11} & D_{12} & 0 \\ D_{12} & D_{22} & 0 \\ 0 & 0 & D_{66} \end{pmatrix}\begin{Bmatrix} -\frac{\partial^2 w_b}{\partial x^2} \\ -\frac{\partial^2 w_b}{\partial y^2} \\ -2\frac{\partial^2 w_b}{\partial x \partial y} \end{Bmatrix} + \begin{pmatrix} D_{11}^s & D_{12}^s & 0 \\ D_{12}^s & D_{22}^s & 0 \\ 0 & 0 & D_{66}^s \end{pmatrix}\begin{Bmatrix} -\frac{\partial^2 w_s}{\partial x^2} \\ -\frac{\partial^2 w_s}{\partial y^2} \\ -2\frac{\partial^2 w_s}{\partial x \partial y} \end{Bmatrix} + \begin{Bmatrix} E_{31}^e \\ E_{31}^e \\ 0 \end{Bmatrix}\phi + \begin{Bmatrix} E_{31}^m \\ E_{31}^m \\ 0 \end{Bmatrix}\gamma \tag{31}$$

$$\begin{Bmatrix} M_x^s \\ M_y^s \\ M_{xy}^s \end{Bmatrix} = \begin{pmatrix} B_{11}^s & B_{12}^s & 0 \\ B_{12}^s & B_{22}^s & 0 \\ 0 & 0 & B_{66}^s \end{pmatrix} \begin{Bmatrix} \frac{\partial u}{\partial x} \\ \frac{\partial v}{\partial y} \\ \frac{\partial u}{\partial y}+\frac{\partial v}{\partial x} \end{Bmatrix} + \begin{pmatrix} D_{11}^s & D_{12}^s & 0 \\ D_{12}^s & D_{22}^s & 0 \\ 0 & 0 & D_{66}^s \end{pmatrix} \begin{Bmatrix} -\frac{\partial^2 w_b}{\partial x^2} \\ -\frac{\partial^2 w_b}{\partial y^2} \\ -2\frac{\partial^2 w_b}{\partial x \partial y} \end{Bmatrix} + \begin{pmatrix} H_{11}^s & H_{12}^s & 0 \\ H_{12}^s & H_{22}^s & 0 \\ 0 & 0 & H_{66}^s \end{pmatrix} \begin{Bmatrix} -\frac{\partial^2 w_s}{\partial x^2} \\ -\frac{\partial^2 w_s}{\partial y^2} \\ -2\frac{\partial^2 w_s}{\partial x \partial y} \end{Bmatrix} + \begin{Bmatrix} F_{31}^e \\ F_{31}^e \\ 0 \end{Bmatrix} \phi + \begin{Bmatrix} F_{31}^m \\ F_{31}^m \\ 0 \end{Bmatrix} \gamma \quad (32)$$

$$\begin{Bmatrix} Q_{xz} \\ Q_{yz} \end{Bmatrix} = \begin{pmatrix} A_{44}^s & 0 \\ 0 & A_{55}^s \end{pmatrix} \begin{Bmatrix} \frac{\partial w_s}{\partial x} \\ \frac{\partial w_s}{\partial y} \end{Bmatrix} - A_{15}^e \begin{Bmatrix} \frac{\partial \phi}{\partial x} \\ \frac{\partial \phi}{\partial y} \end{Bmatrix} - A_{15}^m \begin{Bmatrix} \frac{\partial \gamma}{\partial x} \\ \frac{\partial \gamma}{\partial y} \end{Bmatrix} \quad (33)$$

$$\int_{-h/2}^{h/2} \begin{Bmatrix} D_x \\ D_y \end{Bmatrix} \cos(\xi z) dz = E_{15}^e \begin{Bmatrix} \frac{\partial w_s}{\partial x} \\ \frac{\partial w_s}{\partial y} \end{Bmatrix} + F_{11}^e \begin{Bmatrix} \frac{\partial \phi}{\partial x} \\ \frac{\partial \phi}{\partial y} \end{Bmatrix} + F_{11}^m \begin{Bmatrix} \frac{\partial \gamma}{\partial x} \\ \frac{\partial \gamma}{\partial y} \end{Bmatrix} \quad (34)$$

$$\int_{-h/2}^{h/2} D_z \, \xi \sin(\xi z) dz = A_{31}^e (\frac{\partial u}{\partial x}+\frac{\partial v}{\partial y}) - E_{31}^e \nabla^2 w_b - F_{31}^e \nabla^2 w_s - F_{33}^e \phi - F_{33}^m \gamma \quad (35)$$

$$\int_{-h/2}^{h/2} \begin{Bmatrix} B_x \\ B_y \end{Bmatrix} \cos(\xi z) dz = E_{15}^m \begin{Bmatrix} \frac{\partial w_s}{\partial x} \\ \frac{\partial w_s}{\partial y} \end{Bmatrix} + F_{11}^m \begin{Bmatrix} \frac{\partial \phi}{\partial x} \\ \frac{\partial \phi}{\partial y} \end{Bmatrix} + X_{11}^m \begin{Bmatrix} \frac{\partial \gamma}{\partial x} \\ \frac{\partial \gamma}{\partial y} \end{Bmatrix} \quad (36)$$

$$\int_{-h/2}^{h/2} B_z \, \xi \sin(\xi z) dz = A_{31}^m (\frac{\partial u}{\partial x}+\frac{\partial v}{\partial y}) - E_{31}^m \nabla^2 w_b - F_{31}^m \nabla^2 w_s - F_{33}^m \phi - X_{33}^m \gamma \quad (37)$$

$$\begin{Bmatrix} A_{11}, B_{11}, B_{11}^s, D_{11}, D_{11}^s, H_{11}^s \\ A_{12}, B_{12}, B_{12}^s, D_{12}, D_{12}^s, H_{12}^s \\ A_{66}, B_{66}, B_{66}^s, D_{66}, D_{66}^s, H_{66}^s \end{Bmatrix} = \int_{-h/2}^{h/2} \begin{Bmatrix} \tilde{c}_{66} \\ \tilde{c}_{12} \\ \tilde{c}_{66} \end{Bmatrix} (1, z, f, z^2, z\,f, f^2) dz \;, A_{44}^s = A_{55}^s = \int_{-h/2}^{h/2} \tilde{c}_{55} g^2 dz \quad (38)$$

$$\{A_{31}^e, E_{31}^e, F_{31}^e, A_{31}^m, E_{31}^m, F_{31}^m\} = \sum_{n=1}^{3} \int_{-h_{n-1}}^{h_n} \xi \sin(\xi z)\{e_{31}, e_{31} z\,, e_{31} f, q_{31}, q_{31} z\,, q_{31} f\} dz \quad (39)$$

$$\{A_{15}^e, E_{15}^e, A_{15}^m, E_{15}^m\} = \sum_{n=1}^{3} \int_{-h_{n-1}}^{h_n} \cos(\xi z)\{e_{15}, e_{15} g, q_{15}, q_{15} g\} dz \quad (40)$$

$$\{F_{11}^e, F_{33}^e, F_{11}^m, F_{33}^m\} = \sum_{n=1}^{3} \int_{-h_{n-1}}^{h_n} \{k_{11} \cos^2(\xi z), k_{33} \xi^2 \sin^2(\xi z), d_{11} \cos^2(\xi z), d_{33} \xi^2 \sin^2(\xi z)\} dz \quad (41)$$

$$\{X_{11}^m, X_{33}^m\} = \int_{-h/2}^{h/2} \{\tilde{\chi}_{11} \cos^2(\xi z), \tilde{\chi}_{33} \xi^2 \sin^2(\xi z)\} dz \quad (42)$$

Where $\tilde{c}_{ij}$, $\tilde{e}_{ij}$, $\tilde{q}_{ij}$, $\tilde{d}_{ij}$, $\tilde{k}_{ij}$ and $\tilde{\chi}_{ij}$ are reduced constants for the FG plate under the plane stress state (Ke and Wang 2014) which are given as

$$\{\tilde{c}_{11}, \tilde{c}_{12}\} = \{c_{11}, c_{12}\} - \frac{c_{13}^2}{c_{33}}, \quad \{\tilde{c}_{66}, \tilde{e}_{15}, \tilde{d}_{11}, \tilde{q}_{15}, \tilde{k}_{11}\} = \{c_{66}, e_{15}, d_{11}, q_{15}, k_{11}\}$$

$$\tilde{e}_{31} = e_{31} - \frac{c_{13}e_{33}}{c_{33}}, \tilde{q}_{31} = q_{31} - \frac{c_{13}q_{33}}{c_{33}}, \tilde{d}_{33} = \tilde{d}_{33} + \frac{q_{33}e_{33}}{c_{33}}, \tilde{k}_{33} = k_{33} + \frac{e_{33}^2}{c_{33}}, \tilde{\chi}_{33} = \chi_{33} + \frac{q_{33}^2}{c_{33}}$$
(43)

The governing equations of refined shear deformation MEE porous FG plate in terms of the displacement can be derived by substituting Eqs. (30) -(37), into Eqs. (19) -(24) as follows

$$A_{11}\frac{\partial^2 u}{\partial x^2} + A_{66}\frac{\partial^2 u}{\partial y^2} + (A_{12}+A_{66})\frac{\partial^2 v}{\partial x \partial y} - B_{11}\frac{\partial^3 w_b}{\partial x^3} - (B_{12}+2B_{66})\frac{\partial^3 w_b}{\partial x \partial y^2} - B_{11}^s\frac{\partial^3 w_s}{\partial x^3} - (B_{12}^s+2B_{66}^s)\frac{\partial^3 w_s}{\partial x \partial y^2} + A_{31}^e\frac{\partial \phi}{\partial x} + A_{31}^m\frac{\partial \gamma}{\partial x} = 0 \quad (44)$$

$$A_{66}\frac{\partial^2 v}{\partial x^2} + A_{22}\frac{\partial^2 v}{\partial y^2} + (A_{12}+A_{66})\frac{\partial^2 u}{\partial x \partial y} - B_{22}\frac{\partial^3 w_b}{\partial y^3} - (B_{12}+2B_{66})\frac{\partial^3 w_b}{\partial x^2 \partial y} - B_{22}^s\frac{\partial^3 w_s}{\partial y^3} - (B_{12}^s+2B_{66}^s)\frac{\partial^3 w_s}{\partial x^2 \partial y} + A_{31}^e\frac{\partial \phi}{\partial y} + A_{31}^m\frac{\partial \gamma}{\partial y} = 0 \quad (45)$$

$$B_{11}\frac{\partial^3 u}{\partial x^3} + (B_{12}+2B_{66})\frac{\partial^3 u}{\partial x \partial y^2} + (B_{12}+2B_{66})\frac{\partial^3 v}{\partial x^2 \partial y} + B_{22}\frac{\partial^3 v}{\partial y^3} - D_{11}\frac{\partial^4 w_b}{\partial x^4} + E_{31}^e\nabla^2\phi - 2(D_{12}+2D_{66})\frac{\partial^4 w_b}{\partial x^2 \partial y^2} - D_{22}\frac{\partial^4 w_b}{\partial y^4} - D_{11}^s\frac{\partial^4 w_s}{\partial x^4} -$$
$$2(D_{12}^s+2D_{66}^s)\frac{\partial^4 w_s}{\partial x^2 \partial y^2} + E_{31}^m\nabla^2\gamma - D_{22}^s\frac{\partial^4 w_s}{\partial y^4} - (N^b+N^E+N^H)\nabla^2(w_b+w_s) = 0$$
(46)

$$B_{11}^s\frac{\partial^3 u}{\partial x^3} + (B_{12}^s+2B_{66}^s)\frac{\partial^3 u}{\partial x \partial y^2} + (B_{12}^s+2B_{66}^s)\frac{\partial^3 v}{\partial x^2 \partial y} + B_{22}^s\frac{\partial^3 v}{\partial y^3} - D_{11}^s\frac{\partial^4 w_b}{\partial x^4} + A_{55}^s\frac{\partial^2 w_s}{\partial x^2} + A_{44}^s\frac{\partial^2 w_s}{\partial y^2} - 2(D_{12}^s+2D_{66}^s)\frac{\partial^4 w_b}{\partial x^2 \partial y^2} - D_{22}^s\frac{\partial^4 w_b}{\partial y^4} -$$
$$H_{11}^s\frac{\partial^4 w_s}{\partial x^4} - 2(H_{12}^s+2H_{66}^s)\frac{\partial^4 w_s}{\partial x^2 \partial y^2} - H_{22}^s\frac{\partial^4 w_s}{\partial y^4} + F_{31}^e\nabla^2\phi + F_{31}^m\nabla^2\gamma - (N^b+N^E+N^H)\nabla^2(w_b+w_s) - A_{15}^e\nabla^2\phi - A_{15}^m\nabla^2\gamma = 0$$
(47)

$$A_{31}^e(\frac{\partial u}{\partial x}+\frac{\partial v}{\partial y}) - E_{31}^e\nabla^2 w_b - F_{31}^e\nabla^2 w_s + E_{15}^e\nabla^2 w_s + F_{11}^e\nabla^2\phi + F_{11}^m\nabla^2\gamma - F_{33}^e\phi - F_{33}^m\gamma = 0 \quad (48)$$

$$A_{31}^m(\frac{\partial u}{\partial x}+\frac{\partial v}{\partial y}) - E_{31}^m\nabla^2 w_b - F_{31}^m\nabla^2 w_s + E_{15}^m\nabla^2 w_s + F_{11}^m\nabla^2\phi + X_{11}^m\nabla^2\gamma - F_{33}^m\phi - X_{33}^m\gamma = 0 \quad (49)$$

In this study it assumed that the porous MEE-FG plate is under external electric voltage, magnetic potential and the shear loading is ignored. So $N_{\chi y}^0 = 0$ and $N_\chi^0, N_y^0$ are the normal forces induced by external electric voltage $V$ and external magnetic potential $\Omega$, respectively and are defined as

$$N_x^0 = N_y^0 = N^E + N^H + N^b \quad (50)$$

$$\{N^E, N^H\} = -\int_{-h/2}^{h/2}\{\tilde{e}_{31}V, \tilde{q}_{31}\Omega\}\frac{2}{h}dz \quad (51)$$

## 3. Solution procedure

Table 2 The admissible functions $X_m(x)$ and $Y_n(y)$ (Sobhy 2013)

| Boundary conditions | | The functions $X_m$ and $Y_n$ | |
|---|---|---|---|
| At x=0, a | At y=0, b | $X_m(x)$ | $Y_n(y)$ |
| **SSSS** $X_m(0) = X_m''(0) = 0$ $X_m(a) = X_m''(a) = 0$ | $Y_n(0) = Y_n''(0) = 0$ $Y_n(b) = Y_n''(b) = 0$ | $Sin(\alpha x)$ | $Sin(\beta y)$ |
| **CSSS** $X_m(0) = X_m'(0) = 0$ $X_m(a) = X_m''(a) = 0$ | $Y_n(0) = Y_n''(0) = 0$ $Y_n(b) = Y_n''(b) = 0$ | $Sin(\alpha x)[Cos(\alpha x) - 1]$ | $Sin(\beta y)$ |
| **CSCS** $X_m(0) = X_m'(0) = 0$ $X_m(a) = X_m''(a) = 0$ | $Y_n(0) = Y_n'(0) = 0$ $Y_n(b) = Y_n''(b) = 0$ | $Sin(\alpha x)[Cos(\alpha x) - 1]$ | $Sin(\beta y)[Cos(\beta y) - 1]$ |
| **CCSS** $X_m(0) = X_m'(0) = 0$ $X_m(a) = X_m'(a) = 0$ | $Y_n(0) = Y_n''(0) = 0$ $Y_n(b) = Y_n''(b) = 0$ | $Sin^2(\alpha x)$ | $Sin(\beta y)$ |
| **CCCC** $X_m(0) = X_m'(0) = 0$ $X_m(a) = X_m'(a) = 0$ | $Y_n(0) = Y_n'(0) = 0$ $Y_n(b) = Y_n'(b) = 0$ | $Sin^2(\alpha x)$ | $Sin^2(\beta y)$ |
| **CCFF** $X_m''(0) = X_m'''(0) = 0$ $X_m''(a) = X_m'''(a) = 0$ | $Y_n(0) = Y_n'(0) = 0$ $Y_n(b) = Y_n'(b) = 0$ | $Cos^2(\alpha x)[Sin^2(\alpha x) + 1]$ | $Sin^2(\beta y)$ |

Here, an exact solution of the governing equations for free vibration of a MEE porous FG plate with different boundary conditions is developed. To satisfy boundary conditions, the displacement quantities are presented in the following form

$$u = \sum_{m=1}^{\infty} \sum_{n=1}^{\infty} U_{mn} \frac{\partial X_m(x)}{\partial x} Y_n(y) e^{i\omega_n t} \tag{52}$$

$$v = \sum_{m=1}^{\infty} \sum_{n=1}^{\infty} V_{mn} X_m(x) \frac{\partial Y_n(y)}{\partial y} e^{i\omega_n t} \tag{53}$$

$$\{w_b, w_s\} = \sum_{m=1}^{\infty} \sum_{n=1}^{\infty} \{W_{bmn}, W_{smn}, \Phi_{mn}, \gamma_{mn}\} X_m(x) Y_n(y) e^{i\omega_n t} \tag{54}$$

Where $(U_{mn}, V_{mn}, W_{bmn}, W_{smn}, \Phi_{mn}, \gamma_{mn})$ are the unknown coefficients and the functions $X_m$ and $Y_n$ are tabulated in detail in Table 2 for different boundary conditions ($\alpha=m\pi/a$, $\beta=n\pi/b$). Inserting Eqs. (52)-(54) into Eqs. (44)-(49) respectively, leads to

$$\begin{aligned} &[(A_{11}r_1 + A_{66}r_2)]U_{mn} + (A_{12} + A_{66})r_2 V_{mn} - [B_{11}r_1 + (B_{12} + 2B_{66})r_2]W_{bmn} \\ &+[-(B_{12}^s + 2B_{66}^s)r_2 - B_{11}^s r_1]W_{smn} + A_{31}^e r_{11}\psi_{mn} + A_{31}^m r_{11}\gamma_{mn} = 0 \end{aligned} \tag{55}$$

$$\begin{aligned} &[(A_{12} + A_{66})r_3]U_{mn} + [A_{66}r_3 + A_{22}r_4]V_{mn} + [-B_{22}r_4 - (B_{12} + 2B_{66})r_3]W_{bmn} + \\ &[-B_{22}^s r_4 - (B_{12}^s + 2B_{66}^s)r_1]W_{smn} + A_{31}^e r_{12}\psi_{mn} + A_{31}^m r_{12}\lambda_{mn} = 0 \end{aligned} \tag{56}$$

$$\begin{aligned} &[B_{11}r_5 + (B_{12} + 2B_{66})r_6]U_{mn} + [(B_{12} + 2B_{66})r_6 + B_{22}r_7]V_{mn} + [-D_{11}r_5 - 2(D_{12} + 2D_{66})r_6 - D_{22}r_7 \\ &+(N^E + N^H + N^b)(-(r_{10} + r_9))]W_{bmn} + [-D_{11}^s r_5 - 2(D_{12}^s + 2D_{66}^s)r_6 - D_{22}^s r_7 + \\ &(N^E + N^H + N^b)(-(r_{10} + r_9))]W_{smn} + [E_{31}^e(r_{10} + r_9)]\psi_{mn} + [E_{31}^m(r_9 + r_{10})]\gamma_{mn} = 0 \end{aligned} \tag{57}$$

$[B_{11}^s r_5 + (B_{12}^s + 2B_{66}^s)r_6]U_{mn} + [(B_{12}^s + 2B_{66}^s)r_6 + B_{22}^s r_7]V_{mn} + [-D_{11}^s r_5 - 2(D_{12}^s + 2D_{66}^s)r_6 - D_{22}^s r_7 +$
$(N^E + N^H)(-(r_{10} + r_9))]W_{bmn} + [A_{44}^s(r_{10} + r_9) - H_{11}^s r_5 - 2(H_{12}^s + 2H_{66}^s)r_6 - H_{22}^s r_7 + (N^E + N^H + N^b)$ (58)
$(-(r_{10} + r_9))]W_{smn} + [(F_{31}^e - A_{15}^e)(r_{10} + r_9)]\psi_{mn} + [(F_{31}^m - A_{15}^m)(r_{10} + r_9)]\gamma_{mn} = 0$

$$A_{31}^e r_{10} U_{mn} + A_{31}^e r_9 V_{mn} + [-E_{31}^e(r_{10} + r_9)]W_{bmn} + [(E_{15}^e - F_{31}^e)(r_{10} + r_9)]W_{smn} +$$
$$[F_{11}^e(r_{10} + r_9) - F_{33}^e r_8]\psi_{mn} + [F_{11}^m(r_{10} + r_9) - F_{33}^m r_8]\gamma_{mn} = 0 \tag{59}$$

$$A_{31}^m r_{10} U_{mn} + A_{31}^m r_9 V_{mn} - E_{31}^m(r_{10} + r_9)W_{bmn} + (E_{15}^m - F_{31}^m)(r_{10} + r_9)W_{smn} +$$
$$[F_{11}^m(r_{10} + r_9) - F_{33}^m r_8]\psi_{mn} + [X_{11}^m(r_{10} + r_9) - X_{33}^m r_8]\gamma_{mn} = 0 \tag{60}$$

Where

$$\{r_3, r_4, r_{12}\} = \int_0^a \int_0^b X(x)Y'(y)\{X''(x)Y'(y), X(x)Y'''(y), X(x)Y'(y)\}dxdy \tag{61}$$

$$\{r_1, r_2, r_{11}\} = \int_0^a \int_0^b X'(x)Y(y)\{X'''(x)Y(y), X'(x)Y''(y), X'(x)Y(y)\}dxdy \tag{62}$$

$$\{r_5, r_6, r_7\} = \int_0^a \int_0^b X(x)Y(y)\{X''''(x)Y(y), X''(x)Y''(y), X(x)Y''''(y)\}dxdy \tag{63}$$

$$\{r_8, r_9, r_{10}\} = \int_0^a \int_0^b X(x)Y(y)\{X(x)Y(y), X(x)Y''(y), X''(x)Y(y)\}dxdy \tag{64}$$

By finding determinant of the coefficient matrix of the following equations and setting this multinomial to zero, we can find buckling load.

$$\begin{bmatrix} k_{11} & k_{12} & k_{13} & k_{14} & k_{15} & k_{16} \\ k_{21} & k_{22} & k_{23} & k_{24} & k_{25} & k_{26} \\ k_{31} & k_{32} & k_{33} & k_{34} & k_{35} & k_{36} \\ k_{41} & k_{42} & k_{43} & k_{44} & k_{45} & k_{46} \\ k_{51} & k_{52} & k_{53} & k_{54} & k_{15} & k_{56} \\ k_{61} & k_{62} & k_{63} & k_{64} & k_{65} & k_{66} \end{bmatrix} \begin{bmatrix} U_{mn} \\ V_{mn} \\ W_{bmn} \\ W_{smn} \\ \psi_{mn} \\ \gamma_{mn} \end{bmatrix} = 0 \tag{65}$$

Table 3 Comparison of non-dimensional buckling load of FGM plates ($a=b=10$)

| FSDT (Mohammadi *et al.* 2010) | TSDT (Thai and Choi 2012) | Present ICPT |
|---|---|---|
| | SSSS | |
| $p=0$     18.6854 | 18.6861 | 18.7054 |
| $p=1$     18.8566 | 18.8572 | 18.8735 |
| $p=2$     18.8545 | 18.8021 | 18.8123 |
| | CSCS | |
| $p=0$     33.3206 | 34.1195 | 34.4056 |
| $p=1$     33.9966 | 34.6939 | 34.978 |
| $p=2$     33.9881 | 34.5084 | 34.7691 |

*Farzad Ebrahimi and Ali Jafari*

Table 4 Variation of the dimensionless buckling load of MEE-FG (I)&(II) plate with different electric voltage and porosity volume fractions under various boundary conditions ($\frac{\alpha}{h} = 100, \Omega = 0, P = 2$)

| FG-I | | | | | | | | |
|---|---|---|---|---|---|---|---|---|
| V | SSSS | | | CSSS | | | CCSS | | |
| | $\alpha=0$ | $\alpha=0.1$ | $\alpha=0.2$ | $\alpha=0$ | $\alpha=0.1$ | $\alpha=0.2$ | $\alpha=0$ | $\alpha=0.1$ | $\alpha=0.2$ |
| -500 | 0.92876 | 0.82967 | 0.72971 | 1.43171 | 1.27873 | 1.12447 | 1.72254 | 1.53851 | 1.35305 |
| -250 | 0.91233 | 0.81467 | 0.71618 | 1.41529 | 1.26373 | 1.11095 | 1.70611 | 1.52352 | 1.33953 |
| 0 | 0.89590 | 0.79968 | 0.70266 | 1.39886 | 1.24874 | 1.09742 | 1.68969 | 1.50852 | 1.326 |
| 250 | 0.87948 | 0.78468 | 0.689135 | 1.38243 | 1.23374 | 1.0839 | 1.67326 | 1.49353 | 1.31248 |
| 500 | 0.86305 | 0.76969 | 0.67561 | 1.36601 | 1.21875 | 1.07037 | 1.65683 | 1.47853 | 1.29895 |
| | CSCS | | | CCCC | | | CCFF | | |
| V | $\alpha=0$ | $\alpha=0.1$ | $\alpha=0.2$ | $\alpha=0$ | $\alpha=0.1$ | $\alpha=0.2$ | $\alpha=0$ | $\alpha=0.1$ | $\alpha=0.2$ |
| -500 | 1.84664 | 1.64917 | 1.4501 | 2.35487 | 2.10318 | 1.84961 | 2.79939 | 2.5002 | 2.19885 |
| -250 | 1.83022 | 1.63418 | 1.43658 | 2.33844 | 2.08819 | 1.83609 | 2.78297 | 2.48521 | 2.18533 |
| 0 | 1.81379 | 1.61918 | 1.42305 | 2.32202 | 2.07319 | 1.82256 | 2.76654 | 2.47021 | 2.1718 |
| 250 | 1.79736 | 1.60419 | 1.40953 | 2.30559 | 2.0582 | 1.80904 | 2.75011 | 2.45522 | 2.15828 |
| 500 | 1.78093 | 1.58919 | 1.396 | 2.28916 | 2.0432 | 1.79551 | 2.73368 | 2.44022 | 2.14475 |
| FG-II | | | | | | | | |
| | SSSS | | | CSSS | | | CCSS | | |
| V | $\alpha=0$ | $\alpha=0.1$ | $\alpha=0.2$ | $\alpha=0$ | $\alpha=0.1$ | $\alpha=0.2$ | $\alpha=0$ | $\alpha=0.1$ | $\alpha=0.2$ |
| -500 | 0.928761 | 0.903227 | 0.877596 | 1.43171 | 1.39262 | 1.35339 | 1.72254 | 1.6756 | 1.62848 |
| -250 | 0.912334 | 0.8875 | 0.862577 | 1.41529 | 1.37689 | 1.33837 | 1.70611 | 1.65987 | 1.61346 |
| 0 | 0.895907 | 0.871774 | 0.847558 | 1.39886 | 1.36117 | 1.32335 | 1.68969 | 1.64414 | 1.59844 |
| 250 | 0.87948 | 0.856047 | 0.832539 | 1.38243 | 1.34544 | 1.30833 | 1.67326 | 1.62842 | 1.58343 |
| 500 | 0.863052 | 0.840321 | 0.81752 | 1.36601 | 1.32971 | 1.29331 | 1.65683 | 1.61269 | 1.56841 |
| | CSCS | | | CCCC | | | CCFF | | |
| V | $\alpha=0$ | $\alpha=0.1$ | $\alpha=0.2$ | $\alpha=0$ | $\alpha=0.1$ | $\alpha=0.2$ | $\alpha=0$ | $\alpha=0.1$ | $\alpha=0.2$ |
| -500 | 1.84664 | 1.79636 | 1.7459 | 2.35487 | 2.29086 | 2.22663 | 2.79939 | 2.72337 | 2.64709 |
| -250 | 1.83022 | 1.78063 | 1.73088 | 2.33844 | 2.27514 | 2.21161 | 2.78297 | 2.70765 | 2.63207 |
| 0 | 1.81379 | 1.76491 | 1.71586 | 2.32202 | 2.25941 | 2.19659 | 2.76654 | 2.69192 | 2.61705 |
| 250 | 1.79736 | 1.74918 | 1.70084 | 2.30559 | 2.24368 | 2.18157 | 2.75011 | 2.67619 | 2.60203 |
| 500 | 1.78093 | 1.73345 | 1.68582 | 2.28916 | 2.22796 | 2.16655 | 2.73368 | 2.66047 | 2.58701 |

## 4. Numerical results and discussions

In this section, numerical and graphical examples are presented to examine magneto-electro-mechanical buckling behavior of MEE-FG plates with porosities employing a higher order refined plate theory. So, the influences of porosity volume fraction, FG material graduation, magnetic and electric fields, different types of porosity distributions, various boundary conditions, aspect ratio and side to thickness ratio on the dimensionless buckling load of the MEE porous FG plate will be provided. The correctness of the presented buckling results are compared with those of first and

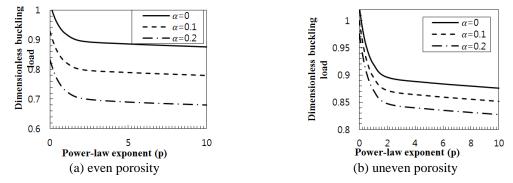(a) even porosity                 (b) uneven porosity

Fig. 3 The variation of the non-dimensional buckling load of SSSS MEE-FG plate with material graduation and porosity parameter for different porosity distribution ($a/h$=100, $\Omega$=0, V=0)



(a) SSSS                      (b) CSSS

(c) CCSS                      (d) CSCS
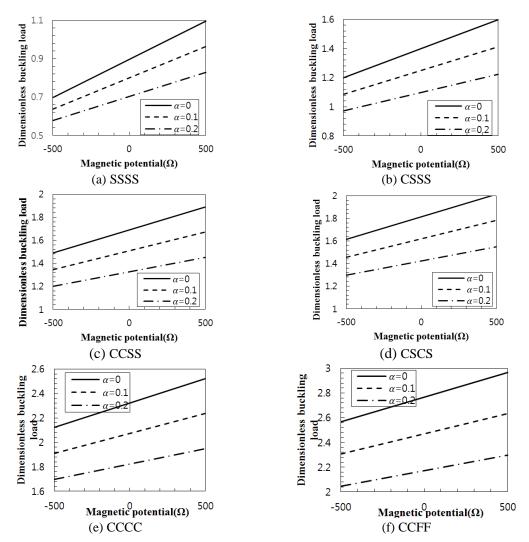
(e) CCCC                      (f) CCFF

Fig. 4 The effect of magnetic potential on the non-dimensional buckling load of MEE-FG-I plate for various boundary conditions and porosity volume fractions ($a/h$=100, V=0, p=2)
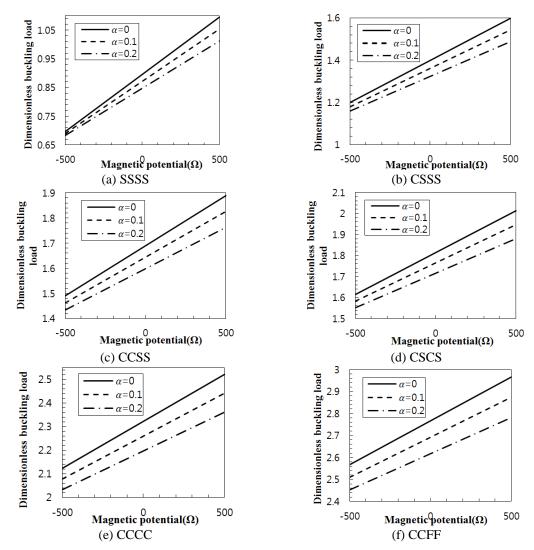
Fig. 5 The effect of magnetic potential on the non-dimensional buckling load of MEE-FG-II plate for various boundary conditions and porosity volume fractions ($a/h$=100, $V$=0, $p$=2)

third order plate theories presented respectively by Mohammadi *et al.* (2010) and Thai and Choi (2012) for a perfect FGM plate and the results are tabulated in Table 3. It is indicated that the present plate model and solution procedure can accurately predict buckling loads of FGM plates. The non-dimensional buckling load ($\overline{N}_{cr}$) can be calculated by the relation in Eq. (66) as

$$\overline{N}_{cr} = N^b \frac{\mathbf{a}^2}{D_c}, D_c = C_{11}^u h^3 \qquad (66)$$

In Table 4, the effect of porosity volume fraction and electric voltage on the non-dimensional buckling load of the MEE-porous FG plates are listed for various boundary conditions (SSSS, CSSS, CCSS, CSCS, CCCC and CCFF), different porosity parameters ($a$=0.0.1,0.2), external

(a) Perfect FGM



(b) Even porosity ($\alpha$=0.2)
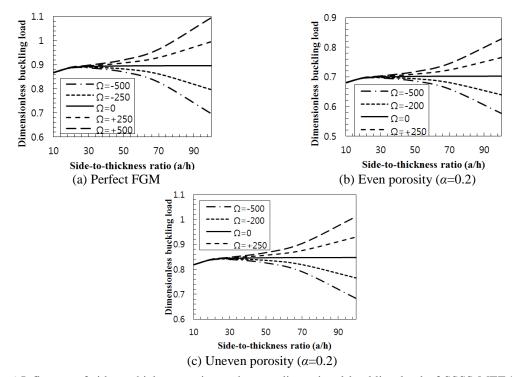


(c) Uneven porosity ($\alpha$=0.2)

Fig. 6 Influence of side-to-thickness ratio on the non-dimensional buckling load of SSSS MEE-FGM square plate for perfect and imperfect (with different porosity distribution) and different magnetic potentials ($p$=2, $V$=0)

electric voltage ($V$=-500, -250, 0, 250, 500) and two porosity distributions (even, uneven) at ($a/h$=100, $\Omega$=0, $P$=0.2). Form the results of this tables, it is concluded that existence of porosity leads substantial reduction on the non-dimensional buckling load of MEE-FG (I)&(II) plate.

Comparing results of even and uneven porosity distributions reveals that the porosity has more considerable impact on the non-dimensional buckling load of the MEE-FG (I) than MEE-FG (II) at every electric voltage. It is seen that external electric voltage has an important role on the buckling behavior of the structure, where the effect of them depends on the sign of electric voltage, in other words negative values of electric voltage leads to increase the non-dimensional buckling load of the smart FG porous plate while, positive values of electric voltage have reverse trend. Comparing the non-dimensional buckling load of smart FG plate for different boundary conditions expresses that the greatest non-dimensional buckling load is obtained for MEE-porous FG plate with CCFF boundary condition followed with other boundary conditions.

In order to peruse the effect of the porosity volume fraction on the non-dimensional buckling load of the smart SSSS&CCCC MEE-FG(I)&(II) plate, the dimensionless buckling load ($N_{cr}$), versus the material graduation index ($p$) for different volume fractions of porosity ($\alpha$=0, 0.1, 0.2) at a constant values of side-to-thickness ratio($a/h$=100), magnetic potential ($\Omega$=0) and electric voltage ($V$=0) is plotted in Fig. 3. It is received that growing of the power-law exponents is cause of reduction in the non-dimensional buckling load of both porosity distributions. The non-dimensional buckling load decreases more intensity where the material graduation is in range from 0 to 2 than that where the material graduation is in range betwixt 2 and 10. In fact, when $p$=0 plate

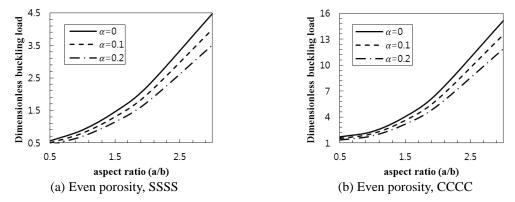(a) Even porosity, SSSS					(b) Even porosity, CCCC

Fig. 7 Effect of aspect ratio on the non-dimensional buckling load of SSSS&CCCC MEE-FG (I)& (II) square plate for different porosity volume fraction ($p$=2, $V$=0, $\Omega$=0)

is made from fully $CoFe_2O_4$ and has the greatest buckling load. Increasing the material graduation exponent from 0 to 10 changes the composition of the MEE-FG plate from a fully $CoFe_2O_4$ plate to a plate with a combination of $CoFe_2O_4$ and $BaTio_3$. So, by increasing the metal percentage and having the lower value of Young's modulus of $BaTio_3$ with respect to $CoFe_2O_4$, the stiffness of system diminishes. Thus, buckling load reduce as the stiffness of a structure decrease.

Also, it is found that the porosity effect on the buckling behavior of smart FG(I)&(II) plate is as follow: The dimensionless buckling load increases as the porosity parameter ($\alpha$) decreases for every value of power-law indexes. Also, it is concluded that the influence of diverse porosity volume fractions on the buckling load of MEE-FG(I) is more tangible than that of the MEE-FG(II). So it is clear that the porosity effect becomes outstanding for MEE-FG plate.

The variations of non-dimensional frequency of MEE-FG(I)&(II) plates versus magnetic potential for various boundary conditions (SSSS, CSSS, CCSS, CSCS, CCCC, CCFF) and different values of porosity volume fractions ($\alpha$=0, 0.1, $\alpha$=0.2), at ($a/h$=100, $p$=2, $V$=0) are plotted in Figs. 4 and 5, respectively. It is found that magnetic potential increasing impacts on the frequency of MEE porous plate when their values vary from negative to positive one at a fixed value of porosity volume fraction which highlights the notability of the sign of magnetic potential. Furthermore, according to these results the non-dimensional buckling load decreases as the porosity value increases for all values of magnetic potential. It is pointed that increasing of the external magnetic potential is cause of increment in buckling load when their values vary from negative to positive one at a fixed value of porosity volume fraction which highlights the notability of the magnitude and sign of magnetic potential.So it is very important to regard the magnetic field in the analysis of MEE-FG plate with porosity. Furthermore, according to these results the non-dimensional buckling load decreases as the porosity value increases for all values of magnetic potential. To display the influence of side-to-thickness ratio on the non-dimensional buckling load of MEE-perfect and imperfect SSSS FG plate for various external magnetic ($\Omega$=500, 250, 0, -250, -500), Fig. 6 presents the dimensionless buckling load results versus side-to-thickness ratio at constant value of power-law index ($p$=2), porosity parameter ($\alpha$=0,0.2), and electric voltage ($V$=0). As can be seen, at first increment of side-thickness ratio leads to increasing of non-dimensional buckling load of MEE-FG(I) for all of the magnetic potentials. Then, with the increasing of a/h, it is seen that $\Omega \succ 0, \Omega = 0, \Omega \prec 0$ provided higher, approximately constant and lower dimensional frequency, respectively.

In addition, it is observable that higher values of *a/h* have more significant influence on frequency response. Consequently, the difference between buckling load results according to negative and positive values of magnetic fields increases with the rise of side-to-thickness ratio.

Fig. 7 show the effect of aspect ratio a/b on the non-dimensional buckling load of smart MEE-FG(I) plate with two boundary conditions (SSSS&CCCC) and porosity parameters ($\alpha$=0, 0.1, 0.2) at (*p*=2, *V*=0, $\Omega$=0). It is pointed that growing of the aspect ratio is cause of increment in the non-dimensional buckling load of MEE-FG plate for both boundary conditions. It can be pointed that the impact of porosity volume fraction on the buckling behavior of MEE-FG plate is similar previous conclusions.

## 5. Conclusions

Based on four-variable higher order shear deformation theory, an analytical method solution is developed for buckling behavior of porous magneto-electro-elastic functionally graded plate with various boundary conditions. Refined shear deformation theory predicts shear deformation effect without any shear correction factors. Magneto electro mechanical characteristics of the smart porous MEE-FG plate are gradually variable in the thickness direction based on modified rule of mixture. The equations of motion and boundary conditions are derived by using Hamilton principle. An analytical solution method is used to solve governing partial differential equations for various boundary conditions. It has been shown that the buckling characteristics of porous MEE-FGM plate are significantly affected by various parameters. Numerical results show that:

• By increasing the material graduation index value, the non-dimensional buckling load of porous MEE-FG plate are found to decrease.

• For MEE-FGM plate with porosities, increasing the volume fraction of porosity first yields a decrease in dimensionless buckling load for both types of porosity distribution.

• Increasing magnetic potential from negative to positive values yields increment of non-dimensional buckling load of porous MEE-FGM plate. However, for the external electric voltage this behavior is opposite.

• The non-dimensional buckling load of porous MEE-FGM plate with CCFF boundary conditions is greatest, followed by CCCC, CSCS, CCSS, CSSS and SSSS respectively.

• Effect of side-to-thickness ratio (*a/h*) on buckling load with respect to magnetic potentials is more prominent at its higher values. As side-to-thickness ratio increases, the difference between buckling load results according to negative and positive values of magnetic fields increases.

• With the increasing of aspect ratio, the non-dimensional buckling load of porous MEE-FG plate increase.

## References

Aghelinejad, M., Zare, K., Ebrahimi, F. and Rastgoo, A. (2011), "Nonlinear thermomechanical post-buckling analysis of thin functionally graded annular plates based on von-karman's plate theory", *Mech. Adv. Mater. Struct.*, **18**(5), 319-326.

Atmane, H.A., Tounsi, A. and Bernard, F. (2015), "Effect of thickness stretching and porosity on mechanical response of a functionally graded beams resting on elastic foundations", *J. Mech. Mater. Des.*, 1-14.

Boutahar, L. and Benamar, R. (2016), "A homogenization procedure for geometrically non-linear free

vibration analysis of functionally graded annular plates with porosities, resting on elastic foundations", *Ain Shams Eng. J.*, **7**(1), 313-333.

Chen, W., Lee, K.Y. and Ding, H. (2005), "On free vibration of non-homogeneous transversely isotropic magneto-electro-elastic plates", *J. Sound Vibr.*, **279**(1), 237-251.

Ebrahimi, F., Ghasemi, F. and Salari, E. (2016), "Investigating thermal effects on vibration behavior of temperature-dependent compositionally graded Euler beams with porosities", *Meccan.*, **51**(1), 223-249.

Ebrahimi, F., Naei, M.H. and Rastgoo, A. (2009), "Geometrically nonlinear vibration analysis of piezoelectrically actuated FGM plate with an initial large deformation", *J. Mech. Sci. Technol.*, **23**(8), 2107-2124.

Ebrahimi, F. and Rastgoo, A. (2011), "Nonlinear vibration analysis of piezo-thermo-electrically actuated functionally graded circular plates", *Arch. Appl. Mech.*, **81**(3), 361-383.

Ebrahimi, F. and Rastgoo, A. (2009), "Nonlinear vibration of smart circular functionally graded plates coupled with piezoelectric layers", *J. Mech. Mater. Des.*, **5**(2), 157-165.

Ebrahimi, F. and Barati, M.R. (2016a), "Temperature distribution effects on buckling behavior of smart heterogeneous nanosize plates based on nonlocal four-variable refined plate theory", *J. Smart Nano Mater.*, **7**(3), 1-25.

Ebrahimi, F. and Barati, M.R. (2016b), "Vibration analysis of smart piezoelectrically actuated nanobeams subjected to magneto-electrical field in thermal environment", *J. Vibr. Contr.*, 1077546316646239.

Ebrahimi, F. and Barati, M.R. (2016c), "Size-dependent thermal stability analysis of graded piezomagnetic nanoplates on elastic medium subjected to various thermal environments", *Appl. Phys. A*, **122**(10), 910.

Ebrahimi, F. and Barati, M.R. (2016d), "Static stability analysis of smart magneto-electro-elastic heterogeneous nanoplates embedded in an elastic medium based on a four-variable refined plate theory", *Smart Mater. Struct.*, **25**(10), 105014.

Ebrahimi, F. and Barati, M.R. (2016e), "Buckling analysis of piezoelectrically actuated smart nanoscale plates subjected to magnetic field", *J. Intell. Mater. Syst. Struct.*, 1045389X16672569.

Ebrahimi, F., Barati, M.R. and Dabbagh, A. (2016), "A nonlocal strain gradient theory for wave propagation analysis in temperature-dependent inhomogeneous nanoplates", *J. Eng. Sci.*, **107**, 169-182.

Ebrahimi, F. and Dabbagh, A. (2016), "On flexural wave propagation responses of smart FG magneto-electro-elastic nanoplates via nonlocal strain gradient theory", *Compos. Struct.*, **162**, 281-293.

Ebrahimi, F. and Hosseini, S.H.S. (2016a), "Thermal effects on nonlinear vibration behavior of viscoelastic nanosize plates", *J. Therm. Str.*, **39**(5), 606-625.

Ebrahimi, F. and Hosseini, S.H.S. (2016b), "Double nanoplate-based NEMS under hydrostatic and electrostatic actuations", *Eur. Phys. J. Plus*, **131**(5), 1-19.

Ebrahimi, F. and Barati, M.R. (2016f), "A nonlocal higher-order shear deformation beam theory for vibration analysis of size-dependent functionally graded nanobeams", *Arab. J. Sci. Eng.*, **41**(5), 1679-1690.

Ebrahimi, F. and Barati, M.R. (2016g), "Vibration analysis of nonlocal beams made of functionally graded material in thermal environment", *Eur. Phys. J. Plus*, **131**(8), 279.

Ebrahimi, F. and Barati, M.R. (2016h), "Dynamic modeling of a thermo-piezo-electrically actuated nanosize beam subjected to a magnetic field", *Appl. Phys. A*, **122**(4), 1-18.

Ebrahimi, F. and Barati, M.R. (2016i), "A unified formulation for dynamic analysis of nonlocal heterogeneous nanobeams in hygro-thermal environment", *Appl. Phys. A*, **122**(9), 792.

Ebrahimi, F. and Barati, M.R. (2016j), "A nonlocal higher-order refined magneto-electro-viscoelastic beam model for dynamic analysis of smart nanostructures", *J. Eng. Sci.*, **107**, 183-196.

Ebrahimi, F. and Barati, M.R. (2016k), "Hygrothermal effects on vibration characteristics of viscoelastic FG nanobeams based on nonlocal strain gradient theory", *Compos. Struct.*, **159**, 433-444.

Ebrahimi, F. and Barati, M.R. (2016l), "Buckling analysis of nonlocal third-order shear deformable functionally graded piezoelectric nanobeams embedded in elastic medium", *J. Brazil. Soc. Mech. Sci. Eng.*, 1-16.

Ebrahimi, F. and Barati, M.R. (2016m), "Magnetic field effects on buckling behavior of smart size-dependent graded nanoscale beams", *Eur. Phys. J. Plus*, **131**(7), 1-14.

Ebrahimi, F. and Barati, M.R. (2016n), "Buckling analysis of smart size-dependent higher order magneto-electro-thermo-elastic functionally graded nanosize beams", *J. Mech.*, 1-11.

Ebrahimi, F. and Barati, M.R. (2017), "A nonlocal strain gradient refined beam model for buckling analysis of size-dependent shear-deformable curved FG nanobeams", *Compos. Struct.*, **159**, 174-182.

Ebrahimi, F., Ghadiri, M., Salari, E., Hoseini, S.A.H. and Shaghaghi, G.R. (2015a), "Application of the differential transformation method for nonlocal vibration analysis of functionally graded nanobeams", *J. Mech. Sci. Technol.*, **29**(3), 1207-1215.

Ebrahimi, F. and Salari, E. (2015a), "Thermal buckling and free vibration analysis of size dependent Timoshenko FG nanobeams in thermal environments", *Compos. Struct.*, **128**, 363-380.

Ebrahimi, F. and Salari, E. (2015b), "Size-dependent free flexural vibrational behavior of functionally graded nanobeams using semi-analytical differential transform method", *Compos. Part B: Eng.*, **79**, 156-169.

Ebrahimi, F. and Salari, E. (2015c), "Nonlocal thermo-mechanical vibration analysis of functionally graded nanobeams in thermal environment", *Acta Astronaut.*, **113**, 29-50.

Ebrahimi, F., Salari, E. and Hosseini, S.A.H. (2015b), "Thermomechanical vibration behavior of FG nanobeams subjected to linear and nonlinear temperature distributions", *J. Therm. Stresses*, **38**(12), 1360-1386.

Ebrahimi, F. and Barati, M.R. (2016o), "An exact solution for buckling analysis of embedded piezoelectro-magnetically actuated nanoscale beams", *Adv. Nano Res.*, **4**(2), 65-84.

Ebrahimi, F. and Barati, M.R. (2016p), "Electromechanical buckling behavior of smart piezoelectrically actuated higher-order size-dependent graded nanoscale beams in thermal environment", *J. Smart Nano Mater.*, **7**(2), 69-90.

Ebrahimi, F. and Barati, M.R. (2016q), "Small scale effects on hygro-thermo-mechanical vibration of temperature dependent nonhomogeneous nanoscale beams", *Mech. Adv. Mater. Struct.*, 1-13.

Ebrahimi, F., Salari, E. and Hosseini, S.A.H. (2016), "In-plane thermal loading effects on vibrational characteristics of functionally graded nanobeams", *Meccan.*, **51**(4), 951-977.

Harshe, G., Dougherty, J. and Newnham, R. (1993), "Theoretical modelling of multilayer magnetoelectric composites", *J. Appl. Electrom. Mater.*, **4**(2), 145-145.

Huang, D., Ding, H. and Chen, W. (2007), "Analytical solution for functionally graded magneto-electro-elastic plane beams", *J. Eng. Sci.*, **45**(2), 467-485.

Jiang, A. and Ding, H. (2004), "Analytical solutions to magneto-electro-elastic beams", *Struct. Eng. Mech.*, **18**(2), 195-209.

Kattimani, S. and Ray, M. (2015), "Control of geometrically nonlinear vibrations of functionally graded magneto-electro-elastic plates", *J. Mech. Sci.*, **99**, 154-167.

Ke, L.L. and Wang, Y.S. (2014), "Free vibration of size-dependent magneto-electro-elastic nanobeams based on the nonlocal theory", *Phys. E: Low-dimens. Syst. Nanostruct.*, **63**, 52-61.

Ke, L.L., Yang, J., Kitipornchai, S. and Bradford, M.A. (2012), "Bending, buckling and vibration of size-dependent functionally graded annular microplates", *Compos. Struct.*, **94**(11), 3250-3257.

Larbi, L.O., Kaci, A., Houari, M.S.A. and Tounsi, A. (2013), "An efficient shear deformation beam theory based on neutral surface position for bending and free vibration of functionally graded beams", *Mech. Based Des. Struct. Mach.*, **41**(4), 421-433.

Liu, M.F. and Chang, T.P. (2010), "Closed form expression for the vibration problem of a transversely isotropic magneto-electro-elastic plate", *J. Appl. Mech.*, **77**(2), 024502.

Mantari, J., Bonilla, E. and Soares, C.G. (2014), "A new tangential-exponential higher order shear deformation theory for advanced composite plates", *Compos. Part B: Eng.*, **60**, 319-328.

Mechab, I., Mechab, B., Benaissa, S., Serier, B. and Bouiadjra, B.B. (2016), "Free vibration analysis of FGM nanoplate with porosities resting on winkler pasternak elastic foundations based on two-variable refined plate theories", *J. Brazil. Soc. Mech. Sci. Eng.*, **38**(8), 1-19.

Mohammadi, M., Saidi, A.R. and Jomehzadeh, E. (2010), "Levy solution for buckling analysis of functionally graded rectangular plates", *Appl. Compos. Mater.*, **17**(2), 81-93.

Nguyen, T.K., Nguyen, T.T.P., Vo, T.P. and Thai, H.T. (2015), "Vibration and buckling analysis of

functionally graded sandwich beams by a new higher-order shear deformation theory", *Compos. Part B: Eng.*, **76**, 273-285.

Pan, E. and Han, F. (2005), "Exact solution for functionally graded and layered magneto-electro-elastic plates", *J. Eng. Sci.*, **43**(3), 321-339.

Ramirez, F., Heyliger, P.R. and Pan, E. (2006), "Free vibration response of two-dimensional magneto-electro-elastic laminated plates", *J. Sound Vibr.*, **292**(3), 626-644.

Rezaei, A. and Saidi, A. (2016), "Application of carrera unified formulation to study the effect of porosity on natural frequencies of thick porous-cellular plates", *Compos. Part B: Eng.*, **91**, 361-370.

Şimşek, M. and Yurtcu, H. (2013), "Analytical solutions for bending and buckling of functionally graded nanobeams based on the nonlocal timoshenko beam theory", *Compos. Struct.*, **97**, 378-386.

Sladek, J., Sladek, V., Krahulec, S., Chen, C. and Young, D. (2015), "Analyses of circular magnetoelectroelastic plates with functionally graded material properties", *Mech. Adv. Mater. Struct.*, **22**(6), 479-489.

Sobhy, M. (2013), "Buckling and free vibration of exponentially graded sandwich plates resting on elastic foundations under various boundary conditions", *Compos. Struct.*, **99**, 76-87.

Thai, H.T. and Choi, D.H. (2012), "An efficient and simple refined theory for buckling analysis of functionally graded plates", *Appl. Math. Model.*, **36**(3), 1008-1022.

Vo, T.P., Thai, H.T., Nguyen, T.K., Inam, F. and Lee, J. (2015), "A quasi-3D theory for vibration and buckling of functionally graded sandwich beams", *Compos. Struct.*, **119**, 1-12.

Wattanasakulpong, N. and Chaikittiratana, A. (2015), "Flexural vibration of imperfect functionally graded beams based on timoshenko beam theory: Chebyshev collocation method", *Meccan.*, **50**(5), 1-12.

Wattanasakulpong, N., Prusty, B.G., Kelly, D.W. and Hoffman, M. (2012), "Free vibration analysis of layered functionally graded beams with experimental validation", *Mater. Des.*, **36**, 182-190.

Wattanasakulpong, N. and Ungbhakorn, V. (2014), "Linear and nonlinear vibration analysis of elastically restrained ends FGM beams with porosities", *Aeros. Sci. Technol.*, **32**(1), 111-120.

Xin, L. and Hu, Z. (2015), "Free vibration of layered magneto-electro-elastic beams by SS-DSC approach", *Compos. Struct.*, **125**, 96-103.

Yahia, S.A., Atmane, H.A., Houari, M.S.A. and Tounsi, A. (2015), "Wave propagation in functionally graded plates with porosities using various higher-order shear deformation plate theories", *Struct. Eng. Mech.*, **53**(6), 1143-1165.

Zeng, X., Yue, Z., Zhao, B. and Wen, S. (2014), "Analysis of a three-dimensional FEM model of a thin piezoelectric actuator embedded in an infinite host structure", *Adv. Mater. Res.*, **3**(1), 237-257.

Zhu, J., Lai, Z., Yin, Z., Jeon, J. and Lee, S. (2001), "Fabrication of ZrO 2-NiCr functionally graded material by powder metallurgy", *Mater. Chem. Phys.*, **68**(1), 130-135.

*OP*